

**Electronic Supplementary Information (ESI):**

**A Rare Case of a Zero-Field Single-Ion Magnet in a  
Cerium(III) Pseudo-Icosahedral Complex**

*Jarrold R. Thomas<sup>a</sup>, Marcus J. Giansiracusa<sup>b\*</sup>, Jonathan T. Mifsud<sup>a</sup>, Richard A. Mole<sup>c</sup>  
and Scott A. Sulway<sup>a\*</sup>*

<sup>a</sup> School of Chemistry, The University of New South Wales (UNSW), Kensington, Sydney, 2052, Australia.

<sup>b</sup> School of Chemistry, University of Melbourne, Parkville, Victoria, 3010, Australia.

<sup>c</sup> The Australian Nuclear Science and Technology Organisation, Lucas Heights, NSW 2232, Australia

\* Corresponding author email: [s.sulway@unsw.edu.au](mailto:s.sulway@unsw.edu.au), [marcus.giansiracusa@unimelb.edu.au](mailto:marcus.giansiracusa@unimelb.edu.au)

## Table of Contents

1. Experimental.....	S3
2. NMR Spectroscopic Data.....	S5
3. FTIR Spectroscopic Data.....	S6
4. Single Crystal XRD Collection, Refined Data, and Images.....	S7
5. Magnetism Data.....	S12
6. <i>Ab initio</i> methods and results.....	S21
7. References.....	S26

## 1. Experimental

### General Procedures

Hydrated lanthanide salts were used as purchased besides that of  $\text{NdCl}_3 \cdot 6\text{H}_2\text{O}$  which was synthesised *via* an acid digestion of  $\text{Nd}_2\text{O}_3$ .<sup>1</sup> KI and solvents were used as purchased. 3-(2'-furyl)-pyrazole and  $\text{KTp}^{2-\text{Fu}}$  were synthesis *via* literature procedures and characterised by newly reported spectroscopic technique.<sup>2,3</sup>  $^1\text{H}$  (400 MHz) and  $^{11}\text{B}$  (128 MHz) NMR data were collected on a 400 MHz Bruker ADVANCED III at 298 K fitted with BBFO temperature probes. Deuterated solvents were purchased through Sigma-Aldrich, dried over 3 Å sieves and degassed. Attenuated Total Reflection-Fourier Transformed Infrared (ATR-FTIR) spectra were collected on a Thermo-scientific Nicolet iS50 using microcrystalline powders in ambient conditions. Elemental analysis was carried out at the Mark Wainwright Analytical Centre (MWAC) XRF laboratory, employing a Elementar varioMACRO cube (CHN).

### Synthesis of $1\text{-Ln} \cdot (\text{CH}_2\text{Cl}_2)_2$ (Ln = La, Ce, Pr, Nd)

**Synthesis of  $[\text{La}(\text{Tp}^{2-\text{Fu}})_2]\text{I} \cdot (\text{CH}_2\text{Cl}_2)_2$  ( $1\text{-La} \cdot (\text{CH}_2\text{Cl}_2)_2$ ).**  $\text{LaCl}_3 \cdot 7\text{H}_2\text{O}$  (0.378 g, 1.02 mmol) and  $\text{KTp}^{2-\text{Fu}}$  (0.912 g, 2.03 mmol) were stirred in methanol (20 ml) for 30 minutes before a methanolic solution (*ca.* 5 ml) of KI (0.166 g, 1.00 mmol) was added slowly. After an hour of stirring the methanol was removed *in vacuo* and replaced with  $\text{CH}_2\text{Cl}_2$  (20 ml), filtered and the resulting solution reduced *in vacuo* yielding a white powder of **1-La** (0.970 g, 0.891 mmol, 89%). Single crystals suitable for X-ray diffraction of **1-La**  $\cdot (\text{CH}_2\text{Cl}_2)_2$  were grown *via* a vapour diffusion of  $\text{Et}_2\text{O}$  into a saturated solution of **1-La** in  $\text{CH}_2\text{Cl}_2$ . Elemental analysis calculated for  $\text{C}_{44}\text{H}_{36}\text{B}_2\text{Cl}_4\text{I}_1\text{La}_1\text{N}_{12}\text{O}_6$ : C 42.01, H 2.88, N 13.36; found: C 42.71, H 2.93, N 13.88. FTIR (ATR, microcrystalline):  $\hat{\nu}$  = 3163 (v. w), 3129 (w), 3079 (w), 3035 (w), 2951 (w), 2501, (w), 2478 (w,  $\nu_{\text{BH}}$  stretch), 2459 (w,  $\nu_{\text{BH}}$  stretch), 1630 (w), 1521 (s), 1489 (s), 1453 (s), 1397 (s), 1387 (s), 1351 (s), 1342 (s), 1269 (s), 1216 (s), 1194 (s), 1154 (s), 1112 (s), 1060 (s), 1043 (s), 1013 (s), 999 (s), 968 (s), 891 (s), 878 (s), 842 (w), 812 (s), 786 (s), 775 (s), 723 (s), 697 (w), 657 (s), 632 (s)  $\text{cm}^{-1}$ .  $^1\text{H}$  (400 MHz,  $d_6$ -DMSO, 298 K):  $\delta$  = 8.22 (d, 6H  $^3J_{\text{HH}}$  = 2.31 Hz, pzH), 6.55 (d, 6H,  $^3J_{\text{HH}}$  = 2.28 Hz, pzH), 6.43 (dd, 6H,  $^3J_{\text{HH}}$  = 3.43 Hz,  $^4J_{\text{HH}}$  = 0.64 Hz, FuH), 6.02 (dd, 6H,  $^3J_{\text{HH}}$  = 3.46 and 2.00 Hz, FuH), 5.75 (s, 4H,  $\text{CH}_2\text{Cl}_2$ ), 4.93 (dd, 6H,  $^3J_{\text{HH}}$  = 1.95 Hz,  $^4J_{\text{HH}}$  = 0.65 Hz, FuH) ppm;  $^{11}\text{B}$  (128 MHz):  $\delta$  = -1.21 (br,  $\nu_{1/2} \approx 420$  Hz, BH borate) ppm.

**Synthesis of  $[\text{Ce}(\text{Tp}^{2-\text{Fu}})_2]\text{I} \cdot (\text{CH}_2\text{Cl}_2)_2$  ( $1\text{-Ce} \cdot (\text{CH}_2\text{Cl}_2)_2$ ).** Method as described for **1-La** with  $\text{CeCl}_3 \cdot 7\text{H}_2\text{O}$  (0.180 g, 0.483 mmol),  $\text{KTp}^{2-\text{Fu}}$  (0.440 g, 0.977 mmol) and KI (84.2 mg, 0.507 mmol), yielding **1-Ce** (0.450 g, 0.401 mmol, 88%) as a white powder. Single crystals suitable for X-ray diffraction of **1-Ce**  $\cdot (\text{CH}_2\text{Cl}_2)_2$  were grown *via* a vapour diffusion of  $\text{Et}_2\text{O}$  into a

saturated solution of **1-Ce** in CH<sub>2</sub>Cl<sub>2</sub>. Elemental analysis calculated for C<sub>44</sub>H<sub>36</sub>B<sub>2</sub>Cl<sub>4</sub>I<sub>1</sub>Ce<sub>1</sub>N<sub>12</sub>O<sub>6</sub>: C 41.97, H 2.88, N 13.36; found: C 42.35, H 2.96, N 13.71. FTIR (ATR, microcrystalline):  $\hat{\nu}$  = 3162 (v. w), 3128 (w), 3079 (w), 3034 (w), 2950 (w), 2502, (w), 2474 (w,  $\nu_{\text{BH}}$  stretch), 2459 (w,  $\nu_{\text{BH}}$  stretch), 1630 (w), 1521 (s), 1489 (s), 1453 (s), 1398 (s), 1387 (s), 1351 (s), 1342 (s), 1269 (s), 1217 (s), 1195 (s), 1155 (s), 1112 (s), 1061 (s), 1043 (s), 1013 (s), 1000 (s), 968 (s), 891 (s), 878 (s), 841 (w), 812 (s), 786 (s), 776 (s), 723 (s), 698 (w), 657 (s), 632 (s) cm<sup>-1</sup>.

**Synthesis of [Pr(Tp<sup>2-Fu</sup>)<sub>2</sub>]**I**·(CH<sub>2</sub>Cl<sub>2</sub>)<sub>2</sub> (**1-Pr**·(CH<sub>2</sub>Cl<sub>2</sub>)<sub>2</sub>).** Method as described for **1-La** with PrCl<sub>3</sub>·6H<sub>2</sub>O (0.357 g, 1.00 mmol), KTp<sup>2-Fu</sup> (0.907 g, 2.01 mmol) and KI (0.166 g, 1.00 mmol), yielding **1-Pr** (0.700 g, 0.640 mmol, 64%) as a white powder. Single crystals suitable for X-ray diffraction of **1-Pr**·(CH<sub>2</sub>Cl<sub>2</sub>)<sub>2</sub> were grown *via* a vapour diffusion of Et<sub>2</sub>O into a saturated solution of **1-Pr** in CH<sub>2</sub>Cl<sub>2</sub>. Elemental analysis calculated for C<sub>44</sub>H<sub>36</sub>B<sub>2</sub>Cl<sub>4</sub>I<sub>1</sub>Pr<sub>1</sub>N<sub>12</sub>O<sub>6</sub>: C 41.94, H 2.88, N 13.34; found: C 42.32, N 3.20, H 13.85. FTIR (ATR, microcrystalline):  $\hat{\nu}$  = 3161 (v. w), 3129 (w), 3080 (w), 3034 (w), 2950 (w), 2503, (w), 2479 (w,  $\nu_{\text{BH}}$  stretch), 2460 (w,  $\nu_{\text{BH}}$  stretch), 1630 (w), 1521 (s), 1490 (s), 1453 (s), 1399 (s), 1388 (s), 1351 (s), 1342 (s), 1270 (s), 1217 (s), 1196 (s), 1156 (s), 1112 (s), 1061 (s), 1044 (s), 1013 (s), 1000 (s), 969 (s), 891 (s), 879 (s), 841 (w), 811 (s), 787 (s), 776 (s), 724 (s), 698 (w), 657 (s), 632 (s) cm<sup>-1</sup>.

**Synthesis of [Nd(Tp<sup>2-Fu</sup>)<sub>2</sub>]**I**·(CH<sub>2</sub>Cl<sub>2</sub>)<sub>2</sub> (**1-Nd**·(CH<sub>2</sub>Cl<sub>2</sub>)<sub>2</sub>).** Method as described for **1-La** with NdCl<sub>3</sub>·6H<sub>2</sub>O (0.360 g, 1.00 mmol), KTp<sup>2-Fu</sup> (0.902 g, 2.00 mmol) and KI (0.166 g, 1.00 mmol), yielding **1-Nd** (0.825 g, 0.752 mmol, 75%) as a white powder. Single crystals suitable for X-ray diffraction of **1-Nd**·(CH<sub>2</sub>Cl<sub>2</sub>)<sub>2</sub> were grown *via* a vapour diffusion of Et<sub>2</sub>O into a saturated solution of **1-Nd** in CH<sub>2</sub>Cl<sub>2</sub>. Elemental analysis calculated for C<sub>44</sub>H<sub>36</sub>B<sub>2</sub>Cl<sub>4</sub>I<sub>1</sub>Nd<sub>1</sub>N<sub>12</sub>O<sub>6</sub>: C 41.83, H 2.87, N 13.30; found: C 42.32, N 3.03, H 13.26. FTIR (ATR, microcrystalline):  $\hat{\nu}$  = 3162 (v. w), 3129 (w), 3080 (w), 3034 (w), 2949 (w), 2504, (w), 2480 (w,  $\nu_{\text{BH}}$  stretch), 2460 (w,  $\nu_{\text{BH}}$  stretch), 1631 (w), 1521 (s), 1491 (s), 1454 (s), 13400 (s), 1388 (s), 1351 (s), 1342 (s), 1270 (s), 1218 (s), 1197 (s), 1157 (s), 1112 (s), 1061 (s), 1043 (s), 1013 (s), 1000 (s), 969 (s), 891 (s), 879 (s), 841 (w), 812 (s), 787 (s), 776 (s), 725 (s), 698 (w), 657 (s), 633 (s) cm<sup>-1</sup>.

## 2. NMR Spectroscopic data

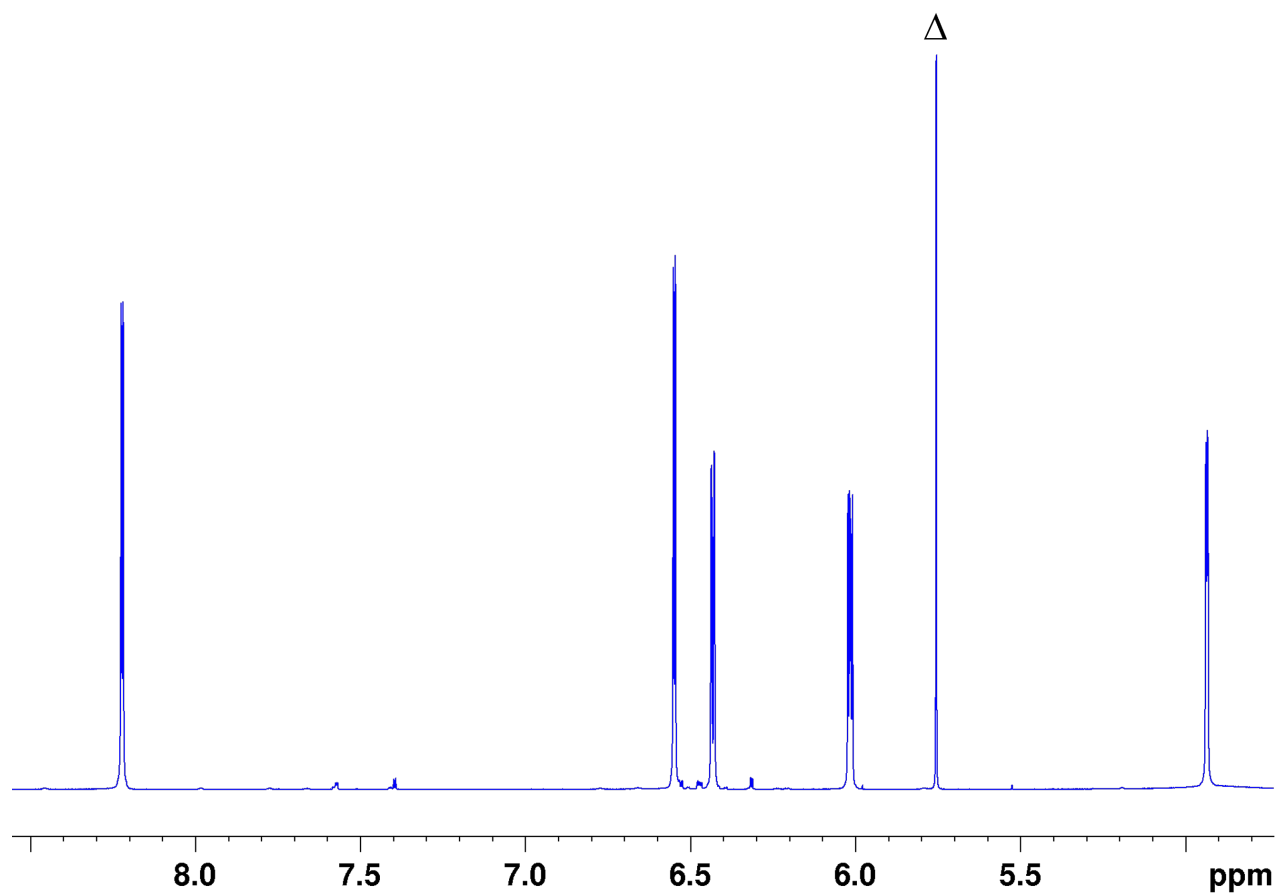


**Figure S1.**  $^1\text{H}$  NMR spectrum of **1-La**· $(\text{CH}_2\text{Cl}_2)_2$  in  $d_6$ -DMSO with included solvent lattice peak of  $\text{CH}_2\text{Cl}_2$  ( $\Delta$ ).

### 3. FTIR Spectroscopic Data

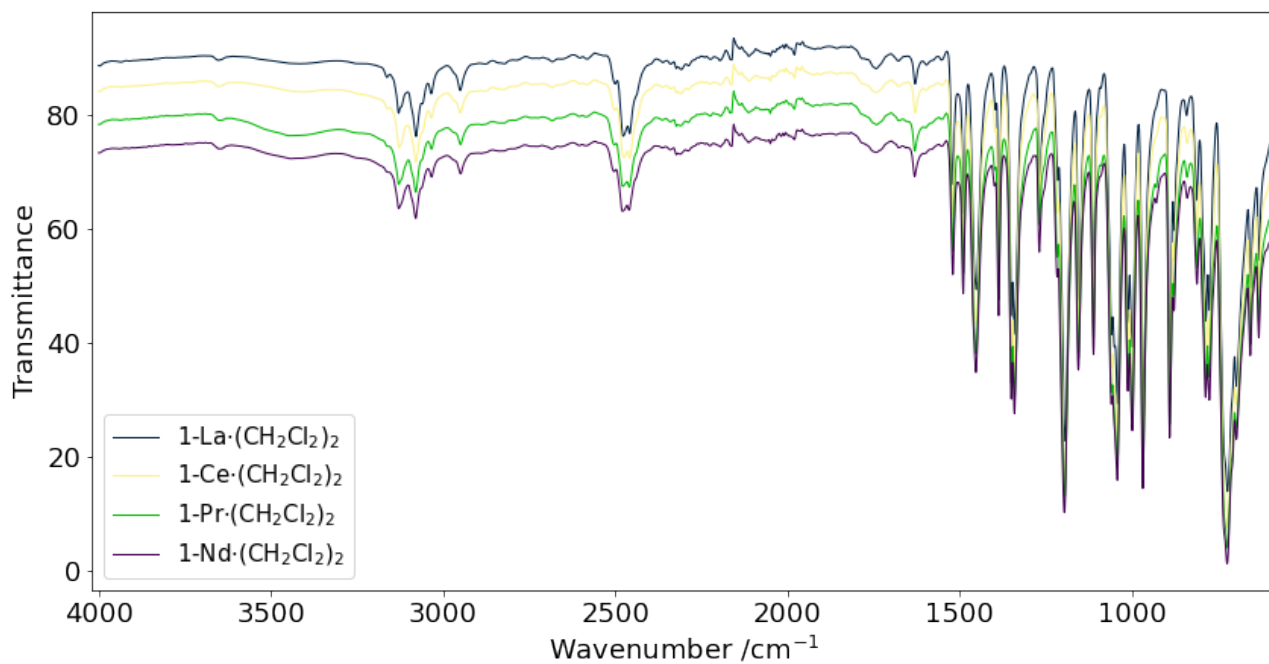


**Figure S2.** ATR FTIR Spectra of **1-Ln**·(CH<sub>2</sub>Cl<sub>2</sub>)<sub>2</sub>. Spectra each been offset by 5% from the previous spectra.

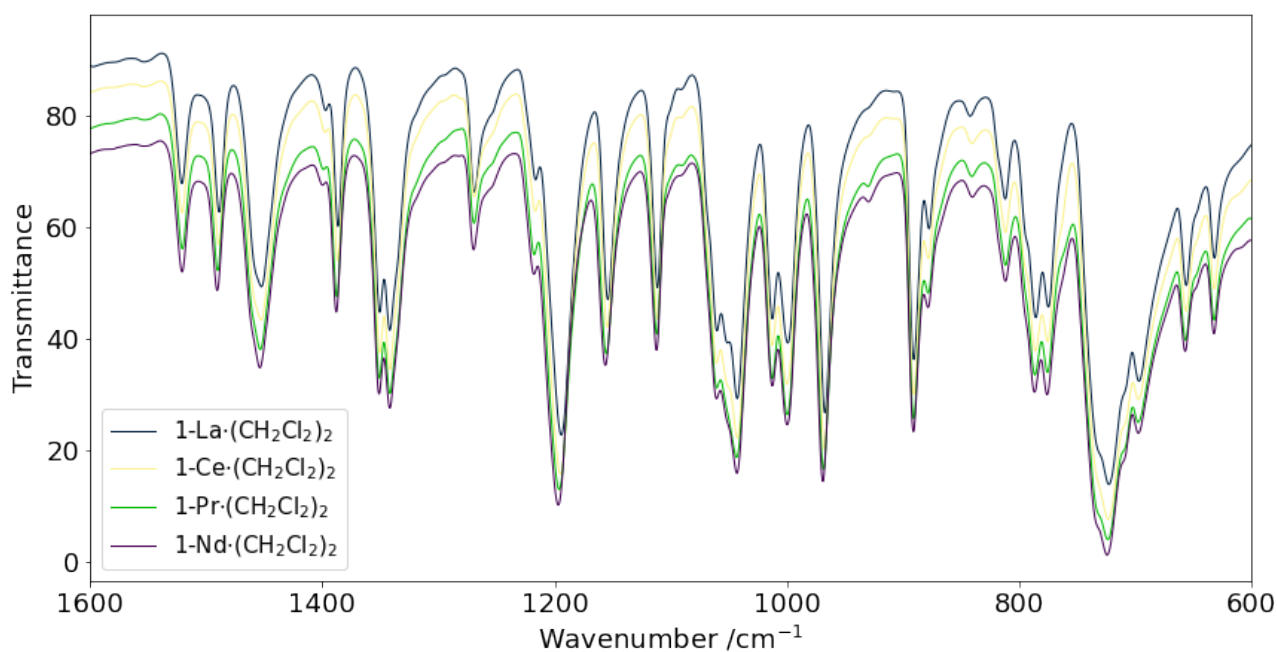


**Figure S3.** ATR FTIR spectra of **1-Ln**·(CH<sub>2</sub>Cl<sub>2</sub>)<sub>2</sub> between 1600 and 600 cm<sup>-1</sup>.

#### 4. Single Crystal XRD Collection, Refined Data, and Images

Single crystal X-ray diffraction data all lanthanide complexes were collected on or a Bruker D8 QUEST diffractometer at 100 K, fitted with a CCD area detector employing a mirror-monochromatic MoK $\alpha$  radiation source ( $\lambda = 0.71073 \text{ \AA}$ ). Integration and scaling data of collections were analysed using APEX5 software. All data was collected with exposures times of 10 seconds with  $1^\circ$  frame sweeps on  $\omega$  and  $\phi$  scans with a detector distance of 45 mm. Multi-scan absorption corrections were used for all compounds. Data was solved in the respective APEX5 software by intrinsic phasing methods using SHELXL.<sup>4</sup> Refinement of crystal data was carried out using least-square refinement methods employed by SHELXT,<sup>5</sup> with all non-hydrogen atoms having anisotropic displacement parameters. Hydrogen atoms were fixed using the riding model. Olex2-1.3<sup>6</sup> was employed for refining data and molecular graphics using postscript image exports. All supplementary crystal data sets can be found on the Cambridge Crystal Data Centre under the codes 2395485-2395488.

**Table S1.** Crystallographic data for compounds **1-Ln**·(CH<sub>2</sub>Cl<sub>2</sub>)<sub>2</sub> (Ln = La, Ce, Pr, Nd).

	<b>1-La·(CH<sub>2</sub>Cl<sub>2</sub>)<sub>2</sub></b>	<b>1-Ce·(CH<sub>2</sub>Cl<sub>2</sub>)<sub>2</sub></b>	<b>1-Pr·(CH<sub>2</sub>Cl<sub>2</sub>)<sub>2</sub></b>	<b>1-Nd·(CH<sub>2</sub>Cl<sub>2</sub>)<sub>2</sub></b>
Systematic Name	[La(Tp <sup>2-Fu</sup> ) <sub>2</sub> ] <sub>2</sub> I·(CH <sub>2</sub> Cl <sub>2</sub> ) <sub>2</sub>	[Ce(Tp <sup>2-Fu</sup> ) <sub>2</sub> ] <sub>2</sub> I·(CH <sub>2</sub> Cl <sub>2</sub> ) <sub>2</sub>	[Pr(Tp <sup>2-Fu</sup> ) <sub>2</sub> ] <sub>2</sub> I·(CH <sub>2</sub> Cl <sub>2</sub> ) <sub>2</sub>	[Nd(Tp <sup>2-Fu</sup> ) <sub>2</sub> ] <sub>2</sub> I·(CH <sub>2</sub> Cl <sub>2</sub> ) <sub>2</sub>
Formula	C <sub>44</sub> H <sub>36</sub> B <sub>2</sub> Cl <sub>4</sub> ILaN <sub>12</sub> O <sub>6</sub>	C <sub>44</sub> H <sub>36</sub> B <sub>2</sub> Cl <sub>4</sub> ICeN <sub>12</sub> O <sub>6</sub>	C <sub>44</sub> H <sub>36</sub> B <sub>2</sub> Cl <sub>4</sub> IPrN <sub>12</sub> O <sub>6</sub>	C <sub>44</sub> H <sub>36</sub> B <sub>2</sub> Cl <sub>4</sub> INdN <sub>12</sub> O <sub>6</sub>
MW/ g mol <sup>-1</sup>	1258.08	1259.29	1260.08	1263.41
Crystal syst	Triclinic	Triclinic	Triclinic	Triclinic
Space Group	<i>P</i> -1	<i>P</i> -1	<i>P</i> -1	<i>P</i> -1
<i>a</i> /Å	11.1211(8)	11.0781(6)	11.0573(5)	11.0672(6)
<i>b</i> /Å	11.3355(7)	11.3685(6)	11.3637(5)	11.3539(7)
<i>c</i> /Å	11.9129(8)	11.8447(6)	11.8627(6)	11.8293(6)
$\alpha$ /°	72.060(3)	72.306(2)	72.195(2)	72.254(2)
$\beta$ /°	69.769(3)	70.058(2)	69.940(2)	70.009(2)
$\gamma$ /°	63.382(2)	63.402(2)	63.419(2)	63.384(2)
<i>V</i> /Å <sup>3</sup>	1238.62(15)	1233.43(12)	1231.40(10)	1228.32(12)
<i>Z</i>	1	1	1	1
$\rho$ /g cm <sup>-3</sup>	1.687	1.695	1.699	1.708
<i>F</i> (000)	620	621	622	623
$\mu$ /mm <sup>-1</sup>	1.761	1.825	1.893	1.963
Reflections Collected	52660	119001	63000	56339
<i>R</i> <sub>int</sub> ( <i>R</i> <sub>s</sub> )	0.0570(0.0296)	0.0527(0.0262)	0.0449(0.0211)	0.0591(0.0299)
Data/Restraints/Parameters	7540/0/319	7501/0/322	7506/0/319	7490/0/319
R indexes ( <i>I</i> ≥ 2σ( <i>I</i> ))	<i>R</i> <sub>1</sub> = 0.0373 <i>wR</i> <sub>2</sub> = 0.0802	<i>R</i> <sub>1</sub> = 0.0283 <i>wR</i> <sub>2</sub> = 0.0705	<i>R</i> <sub>1</sub> = 0.0232 <i>wR</i> <sub>2</sub> = 0.0511	<i>R</i> <sub>1</sub> = 0.0326 <i>wR</i> <sub>2</sub> = 0.0723
R indexes (all data)	<i>R</i> <sub>1</sub> = 0.0464 <i>wR</i> <sub>2</sub> = 0.0885	<i>R</i> <sub>1</sub> = 0.0308 <i>wR</i> <sub>2</sub> = 0.0738	<i>R</i> <sub>1</sub> = 0.0279 <i>wR</i> <sub>2</sub> = 0.0555	<i>R</i> <sub>1</sub> = 0.0399 <i>wR</i> <sub>2</sub> = 0.0796
Diff. peak/hole /e Å <sup>-3</sup>	1.08/-1.77	0.95/-1.59	0.71/-0.96	0.96/-1.65
Goodness-of-fit on <i>F</i> <sup>2</sup>	1.190	1.109	1.187	1.156



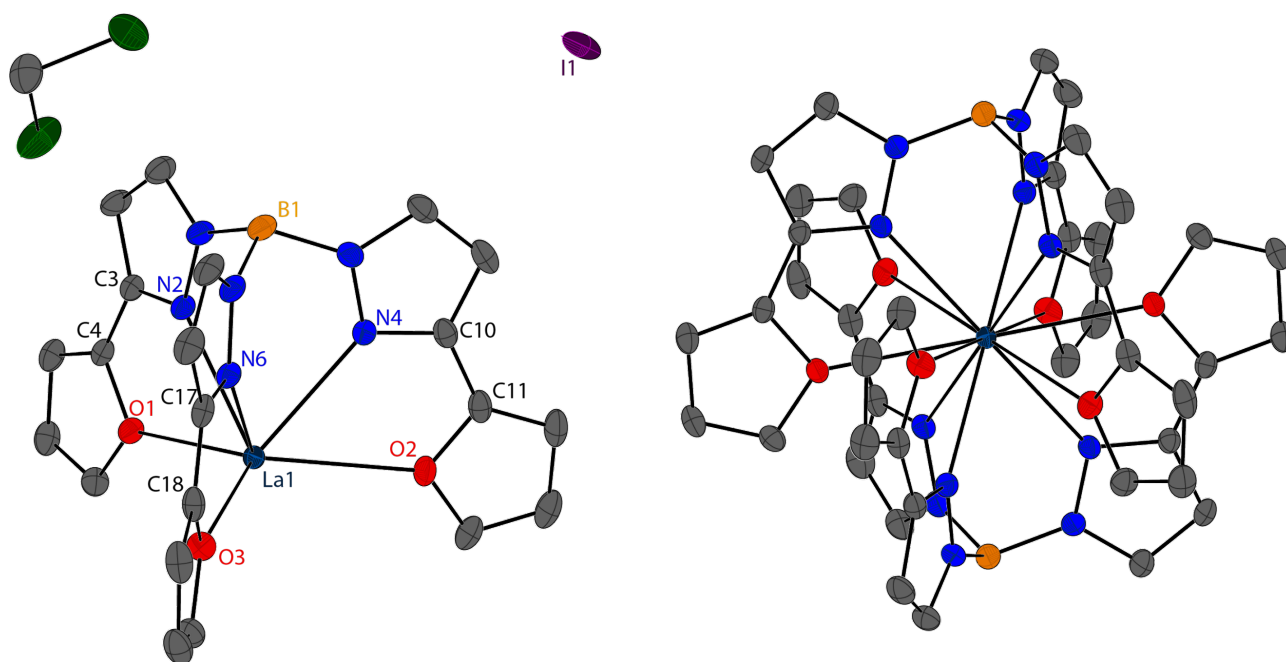


**Figure S4.** Solid-state structures asymmetric unit (left) and the cation (right) in **1-La**·(CH<sub>2</sub>Cl<sub>2</sub>)<sub>2</sub>, drawn with 50% ellipsoid. Lanthanum(III) = navy, iodine = purple, oxygen = red, nitrogen = blue, carbon = grey, boron = orange, hydrogen atoms and lattice solvents have been omitted for clarity.

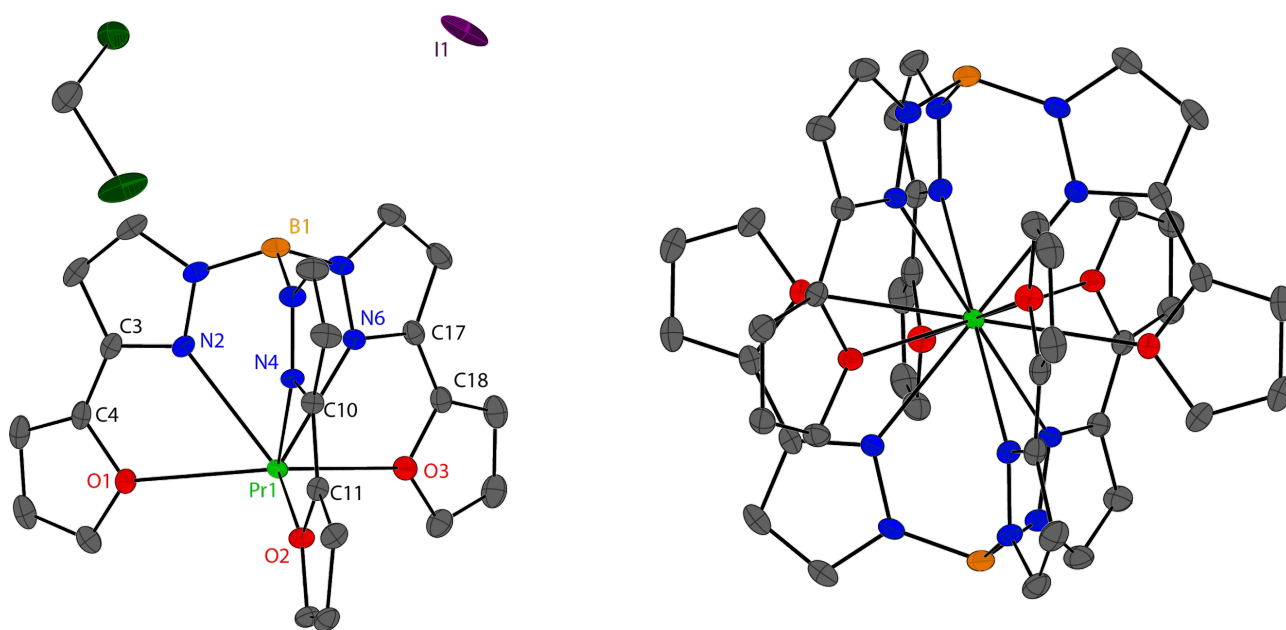


**Figure S5.** Solid-state structures asymmetric unit (left) and the cation (right) in **1-Pr**·(CH<sub>2</sub>Cl<sub>2</sub>)<sub>2</sub>, drawn with 50% ellipsoid. Praseodymium(III) = light green, iodine = purple, oxygen = red, nitrogen = blue, carbon = grey, boron = orange, hydrogen atoms and lattice solvents have been omitted for clarity.

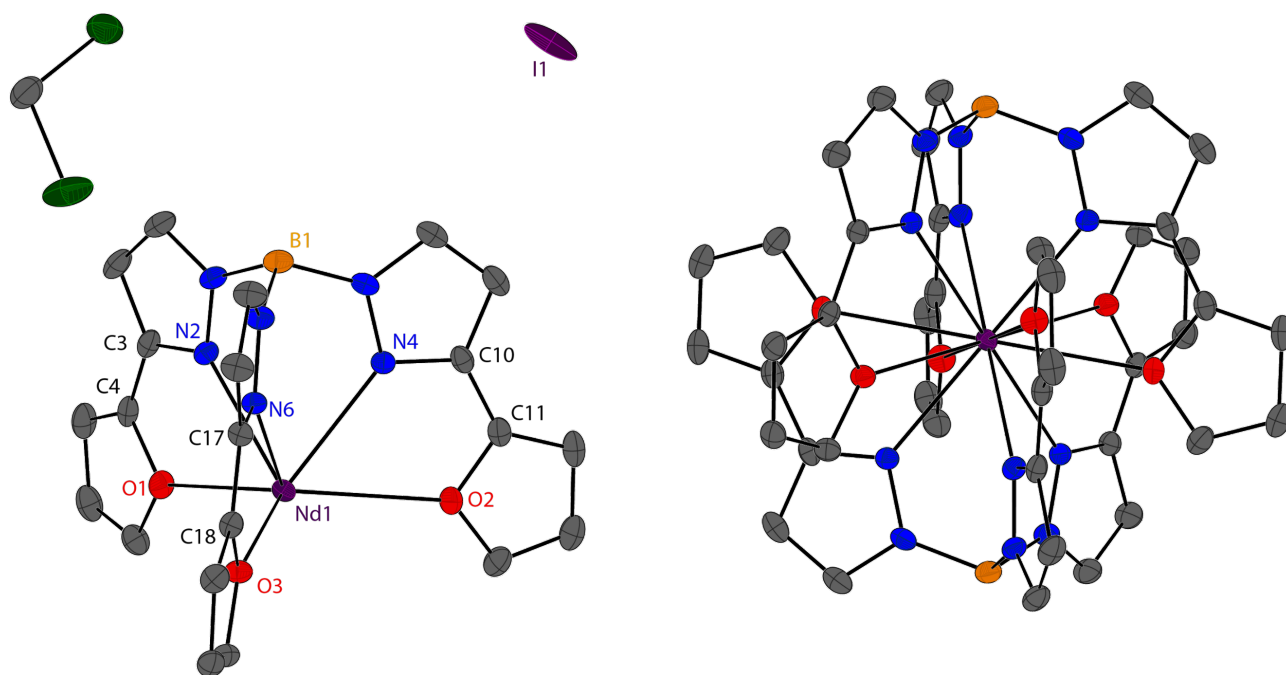


**Figure S6.** Solid-state structures asymmetric unit (left) and the cation (right) in **1-Nd**·(CH<sub>2</sub>Cl<sub>2</sub>)<sub>2</sub>, drawn with 50% ellipsoid. Neodymium(III) = dark purple, iodine = purple, chlorine = dark green, oxygen = red, nitrogen = blue, carbon = grey, boron = orange, hydrogen atoms and lattice solvents have been omitted for clarity.

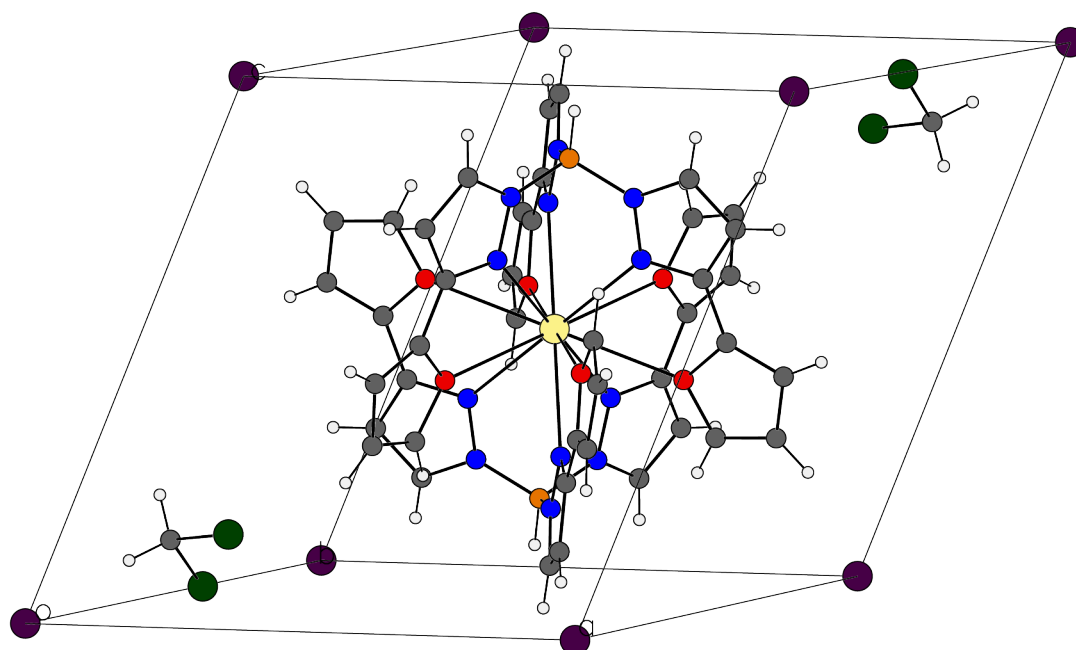


**Figure S7.** Example of unit cell for **1-Ln** shown with **1-Ce**, where the one cation resides within the unit cell, iodide atoms occupying the corners of the cell and CH<sub>2</sub>Cl<sub>2</sub> molecules in the voids between these. Colour scheme follows that established in Figure 1, with hydrogen atoms shown in white.

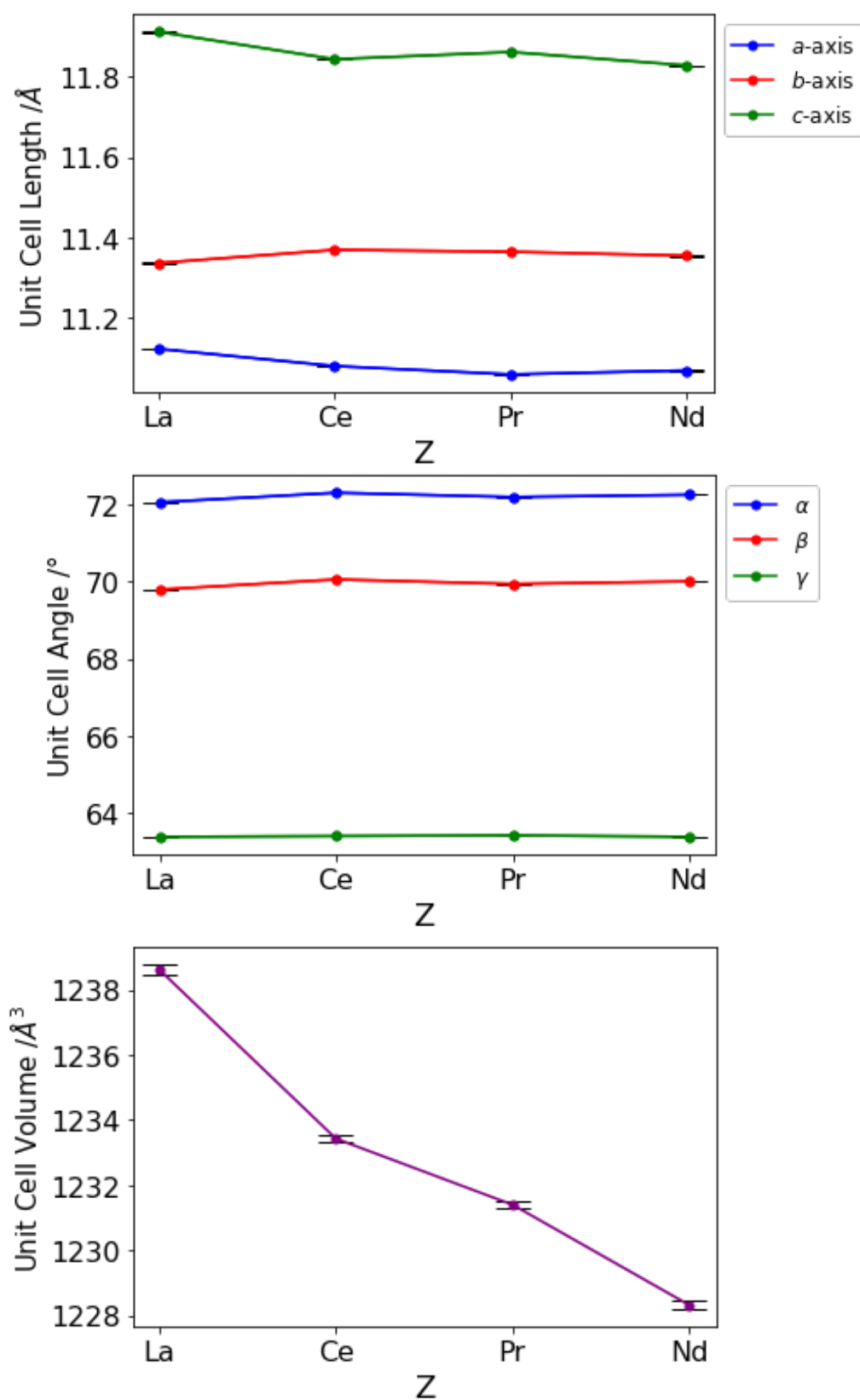


**Figure S8.** Crystallographic data **1-Ln**; Unit cell length (top), angles(middle) and volume (bottom) with ESD's shown as black error bars.

## 5. Magnetic Data

Magnetic measurements were carried out using a Quantum Design PPMS (10-10,000 Hz) magnetometer and Quantum Design MPMS3 Superconducting Quantum Interference Device (SQUID) (0.1 – 1000 Hz). DC measurements were conducted using vibrating sample magnetometry (VSM) on powder sample restrained in eicosane inside gel capsules suspended in straws. Magnetic susceptibility data were collected from 1.8 to 300 K with an average sweep rate of 5 K/min. Magnetisation curves were collected from 0 to 7 T at 2, 4 and 6 K and hysteresis data collected with an average sweep rate of 25 Oe/s. AC magnetic data was collected with ACMS module fitted with an oscillating magnetic field of  $H_{ac} = 5$  Oe (PPMS) or 2 Oe (MPMS). In phase ( $\chi'$ ) an out-of-phase ( $\chi''$ ) magnetic susceptibility for **1-Ce** were initially collected in zero-applied fields ( $H_{dc} = 0$  Oe) between 2-20 K on the PPMS. Once temperature dependence was determined, zero-applied field  $\chi'$  and  $\chi''$  were measured between 0.1-900 Hz on the MPMS, where the  $\chi''$  was fitted to the generalised Debye model using Equation S1. Applied field sweeps at 2 K were performed for 1-Ln to determine the optimal applied fields for magnetic relaxation. Optimal applied fields for **1-Ce** and **1-Nd** were 250 Oe and 2000 Oe, respectively, and regardless of applied field no peaks in  $\chi''$  were observed for **1-Pr**. Magnetic relaxation times were fit using Equations S2 to determine magnetic relaxation mechanisms.

$$\chi'' = (\chi_T - \chi_S) \frac{\cos\left(\frac{\pi\alpha}{2}\right)(\omega\tau)^{1-\alpha}}{1 + 2\sin\left(\frac{\pi\alpha}{2}\right)(\omega\tau)^{1-\alpha} + (\omega\tau)^{2-2\alpha}} \quad (S1)$$

$$\tau^{-1} = \tau_0^{-1} \exp\left(-\frac{U_{eff}}{k_B T}\right) + CT^n \quad (S2)$$

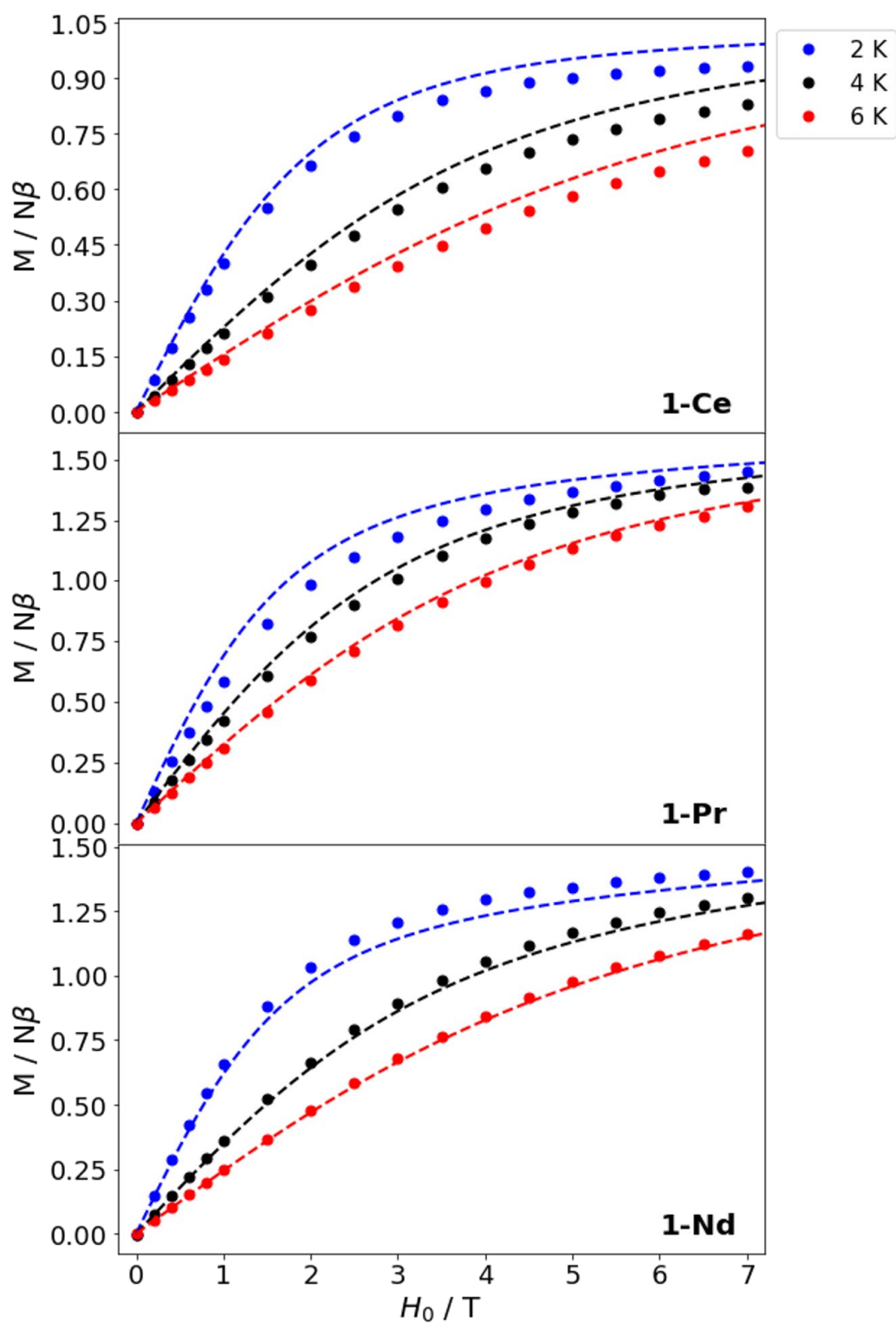


**Figure S9.** Magnetisation Curves for **1-Ln** (top, Ln = Ce; middle, Ln = Pr; bottom, Ln = Nd), at 2 (blue), 4 (black) and 6 (red) K. Points are experimental data and dashed lines are from CASSCF calculations.

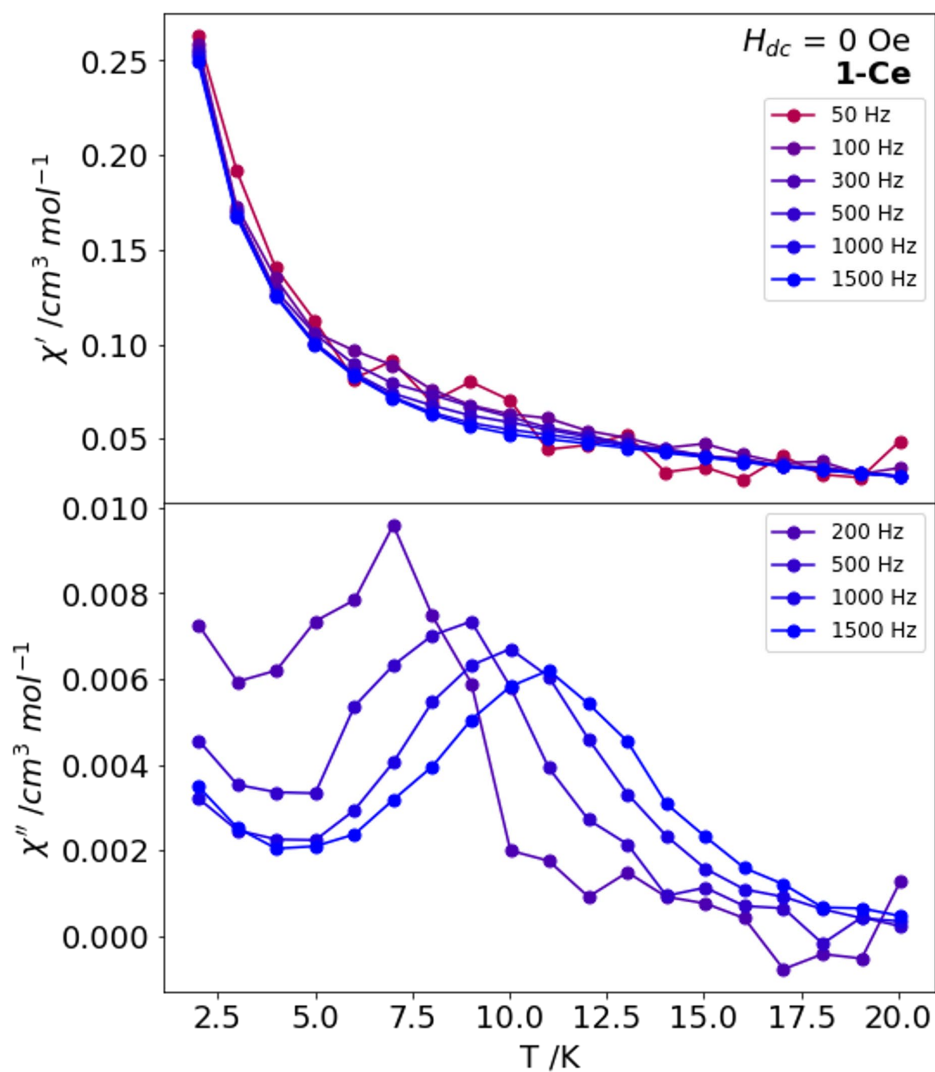


**Figure S10.** Zero-field ac magnetic susceptibility of **1-Ce** collect on the PPMS to identify magnetic behaviour.

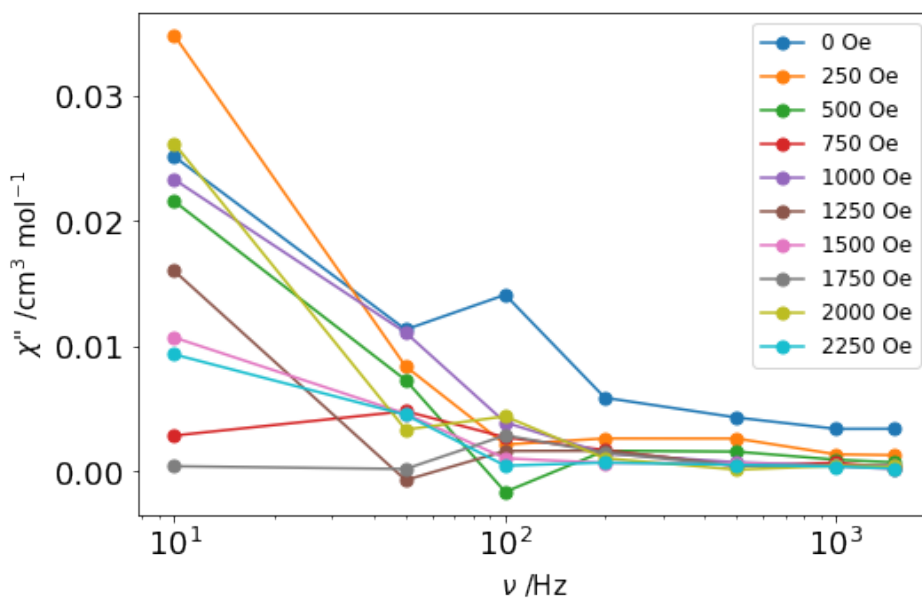


**Figure S11.** Applied-field sweep at  $T = 2$  K for **1-Ce** to identify optimal applied-field. In this case the optimal field chosen was  $H_{dc} = 250$  Oe.

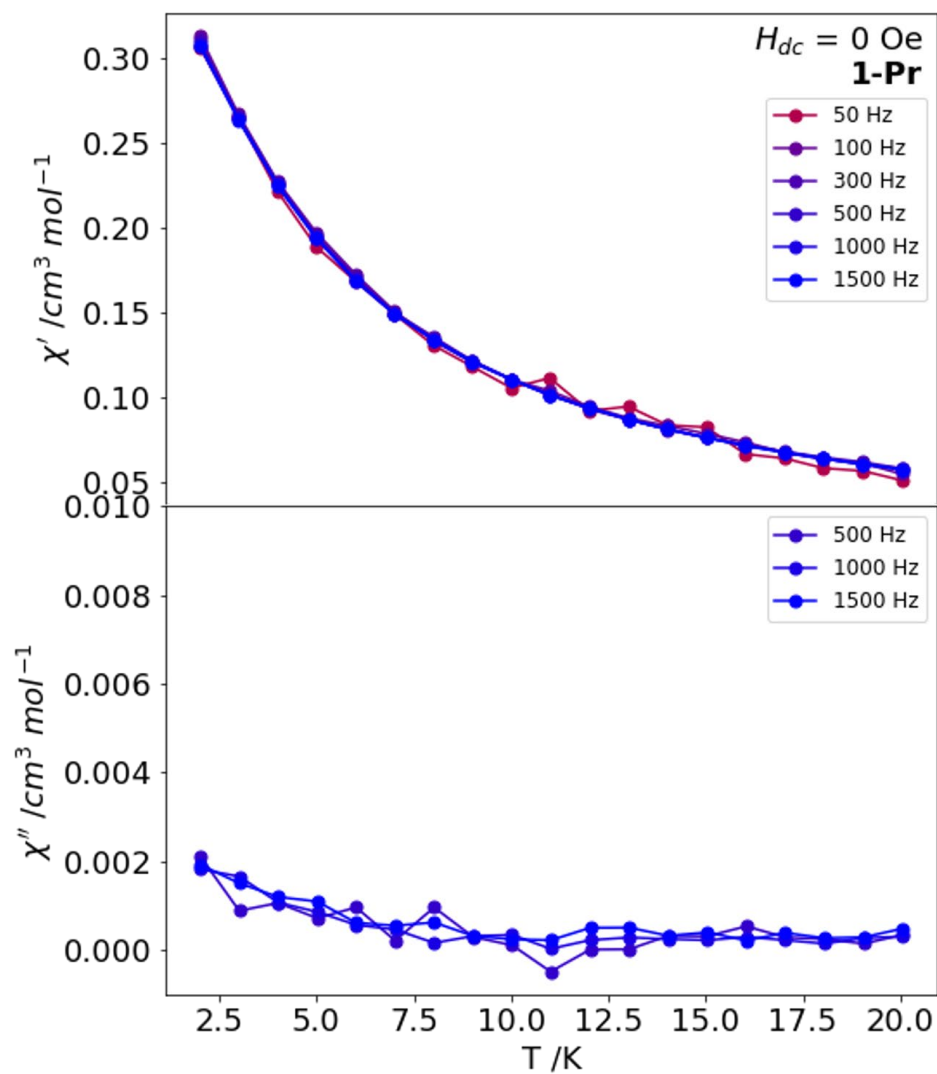


**Figure S12.** Zero-field ac magnetic susceptibility of **1-Pr** collect on the PPMS to identify magnetic behaviour.

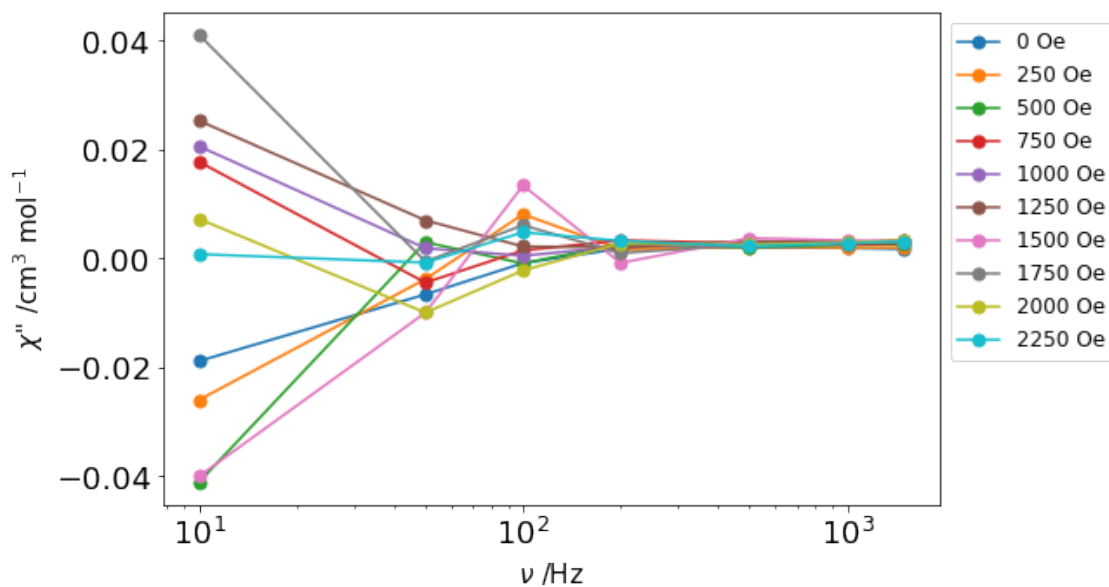


**Figure S13.** Applied-field sweep at  $T = 2$  K for **1-Pr** to identify optimal applied-field. In this case no optimal field was chosen.

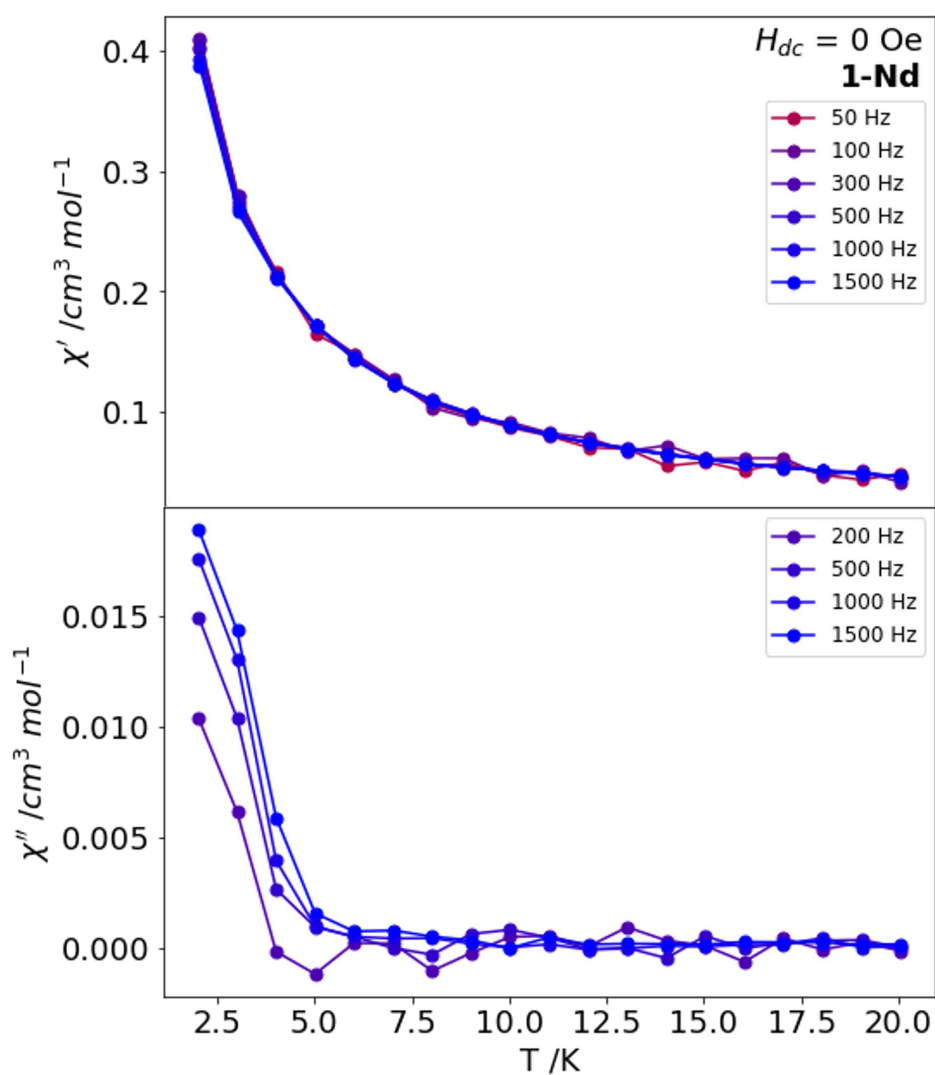


**Figure S14.** Zero-field ac magnetic susceptibility of **1-Nd** collect on the PPMS to identify magnetic behaviour.

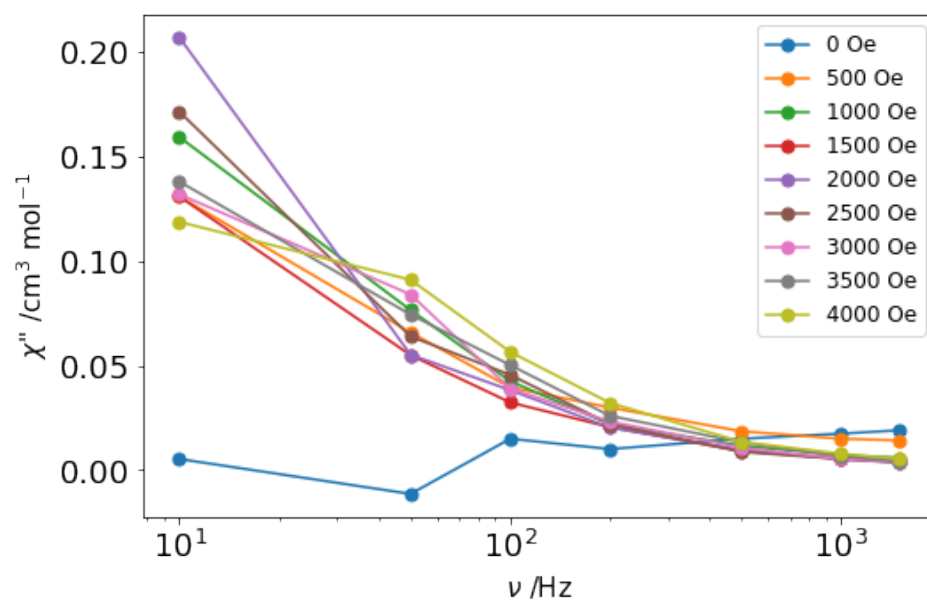


**Figure S15.** Applied-field sweep at  $T = 2$  K for **1-Nd** to identify optimal applied-field. In this case the optimal field chosen was  $H_{dc} = 2000$  Oe.



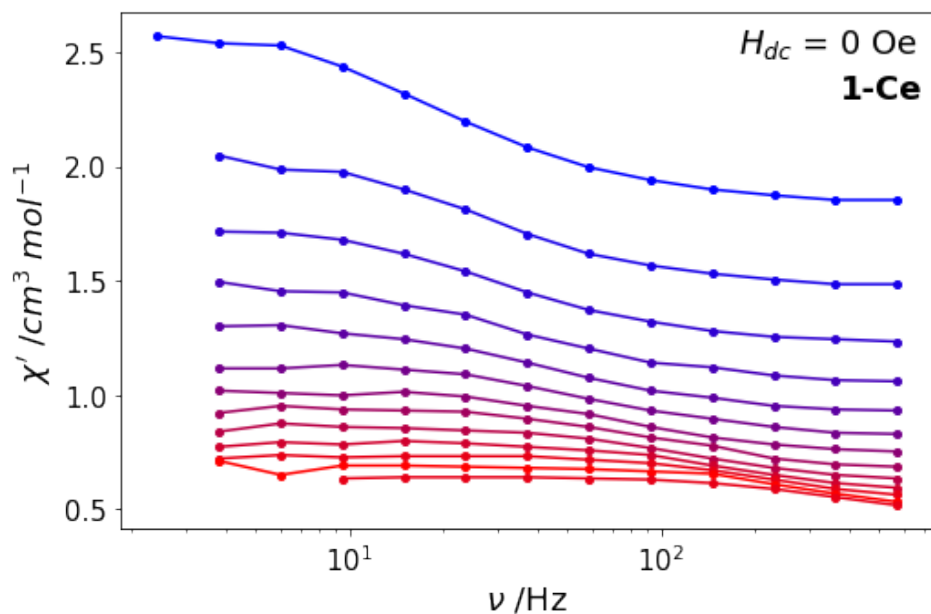


**Figure S16.** Zero-field in phase magnetic susceptibility ( $\chi'$ ) for **1-Ce** collected between 2 (blue) and 8 (red) K. Solid lines are guides for the eye.

**Table S2.** Fitted parameters to the generalised Debye equation for **1-Ce** in zero-field, extracted from  $\chi''$  between 2 K and 8 K with residual sum of squares values ( $R^2$ ) per fit.

$T / \text{K}$	$\alpha$	$\tau / \text{s}$	$\chi_{\text{S}} / \text{cm}^3 \text{mol}^{-1}$	$\chi_{\text{T}} / \text{cm}^3 \text{mol}^{-1}$	$R^2$
2.0	0.118128	0.007797	0.636056	1.400454	0.951358
2.5	0.113694	0.00577	0.361518	0.947581	0.983645
3.0	0.092098	0.0048	0.33081	0.825265	0.975844
3.5	0.113013	0.003904	0.285897	0.714203	0.948927
4.0	0.089011	0.003284	0.31343	0.686798	0.929614
4.5	0.095375	0.002498	0.330682	0.668159	0.965247
5.0	0.086425	0.002129	0.352233	0.648366	0.925778
5.5	0.02539	0.001627	0.361777	0.6187	0.916582
6.0	0.104222	0.001216	0.376443	0.625074	0.957662
6.5	1.62E-15	0.000924	0.394759	0.60501	0.983604
7.0	0.048095	0.000705	0.394523	0.605479	0.93053
7.5	0.018513	0.000525	0.405465	0.594288	0.980634
8.0	0.073463	0.000371	0.004341	0.19566	0.986815

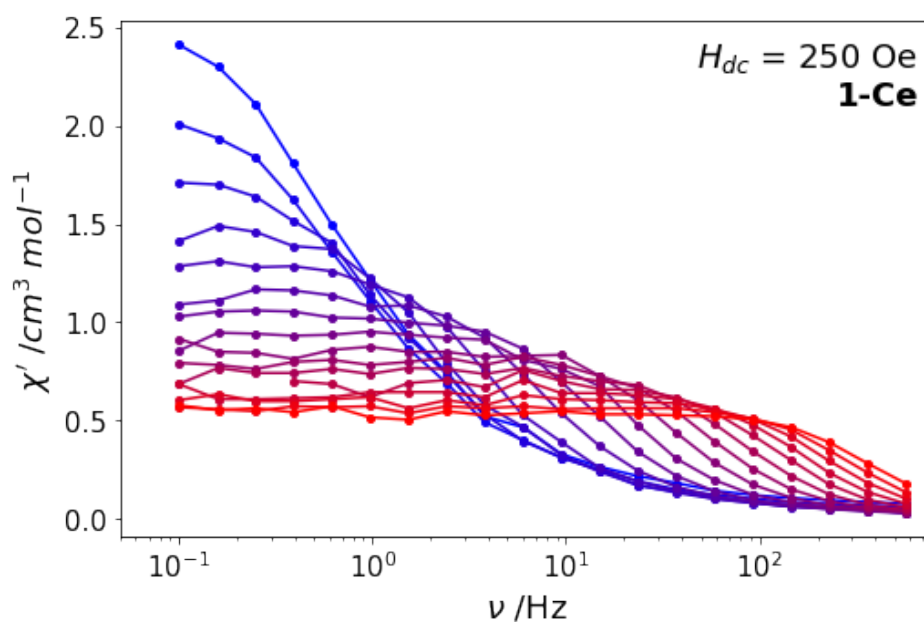


**Figure S17.** Applied-field ( $H_{dc} = 250$  Oe) in phase magnetic susceptibility ( $\chi'$ ) for **1-Ce** collected between 2 (blue) and 9.5 (red) K. Solid lines are guides for the eye.

**Table S3.** Fitted parameters to the generalised Debye equation for **1-Ce** in an applied field of  $H_{dc} = 250$  Oe, extracted from  $\chi''$  between 2 K and 9.5 K with residual sum of squares values ( $R^2$ ) per fit.

$T / \text{K}$	$\alpha$	$\tau / \text{s}$	$\chi_s / \text{cm}^3 \text{mol}^{-1}$	$\chi_T / \text{cm}^3 \text{mol}^{-1}$	$R^2$
2.0	0.302238	0.228328	0.154605	2.811384	0.992922
2.5	0.273258	0.156422	0.336134	2.416516	0.987407
3.0	0.224104	0.098641	0.663098	2.432825	0.98913
3.5	0.173734	0.059152	0.723399	2.190119	0.990084
4.0	0.134352	0.03351	0.231004	1.511455	0.991605
4.5	0.103175	0.019372	0.436031	1.570877	0.985516
5.0	0.093646	0.011115	0.510566	1.529332	0.994681
5.5	0.046168	0.006285	0.057551	0.933664	0.994087
6.0	0.058282	0.00422	0.078593	0.923454	0.932455
6.5	0.063905	0.0028	0.098835	0.890257	0.983039
7.0	0.02676	0.001846	0.14936	0.852015	0.987485
7.5	0.070526	0.001338	0.6454	1.330899	0.967804
8.0	0.070847	0.000944	0.161407	0.820093	0.862296
8.5	0.014026	0.000716	0.204841	0.795084	0.935563
9.0	0.028083	0.000545	0.218061	0.781963	0.973435
9.5	0.019717	0.000418	0.231971	0.768636	0.964888

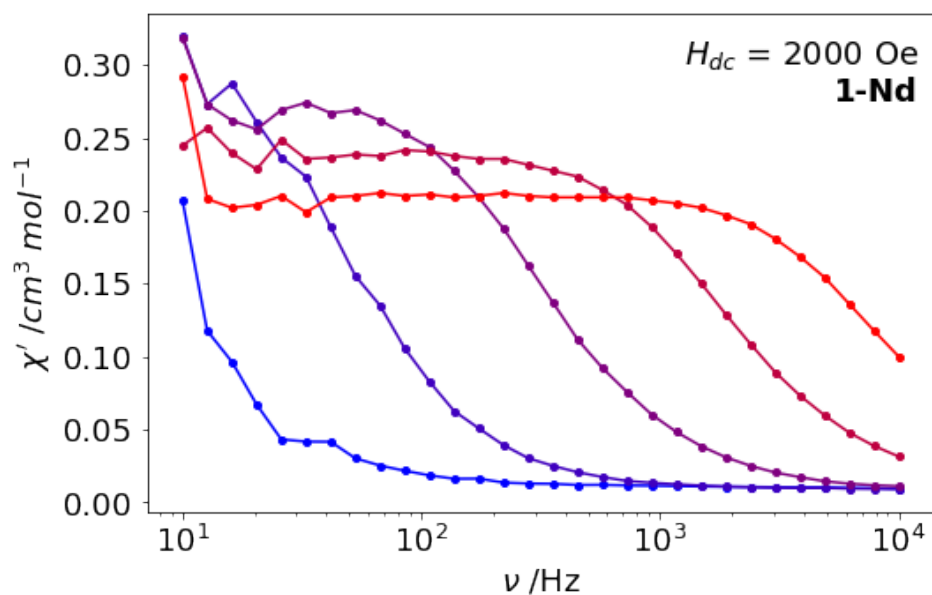


**Figure S18.** Applied-field ( $H_{dc} = 2000$  Oe) in phase magnetic susceptibility ( $\chi'$ ) for **1-Nd** collected between 2 (blue) and 4 (red) K. Solid lines are guides for the eye.

**Table S4.** Fitted parameters to the generalised Debye equation for **1-Ce** in an applied field of  $H_{dc} = 250$  Oe, extracted from  $\chi''$  between 2 K and 9.5 K with residual sum of squares values ( $R^2$ ) per fit.

$T / K$	$\alpha$	$\tau / s$	$\chi_S / \text{cm}^3 \text{mol}^{-1}$	$\chi_T / \text{cm}^3 \text{mol}^{-1}$	$R^2$
2.0	0.077619	0.018981	2.061713	2.439629	0.98321
2.5	0.04944	0.00292	2.106439	2.40398	0.952408
3.0	0.081957	0.000453	2.104986	2.369541	0.963223
3.5	0.073093	8.08E-05	2.026676	2.253736	0.890687
4.0	0.054787	2.08E-05	2.144226	2.332475	0.965725

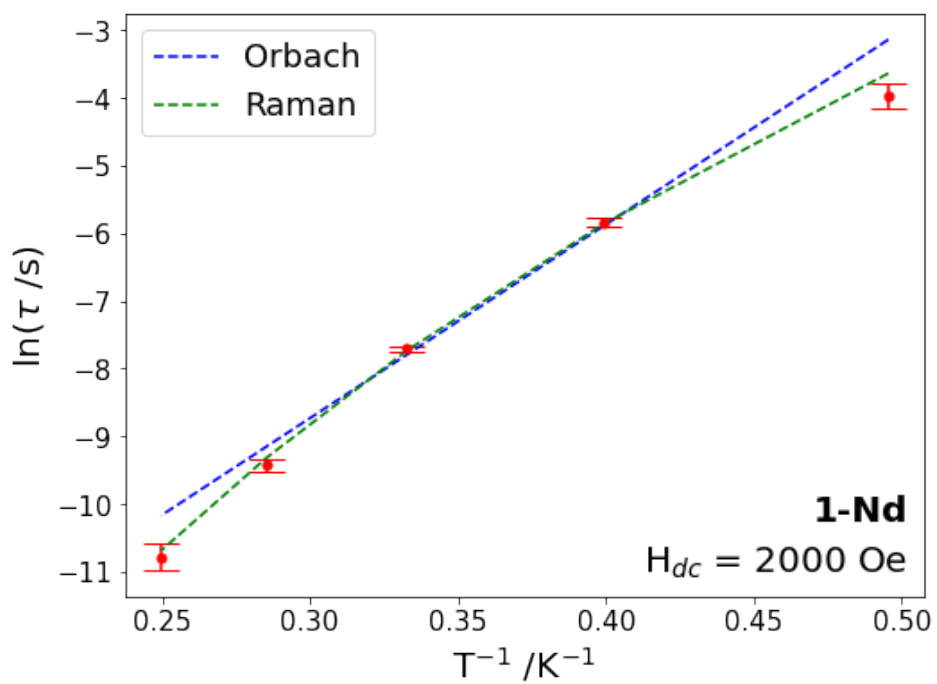


**Figure S19.** Magnetic relaxation plot for **1-Nd** from data collected in an applied field of  $H_{dc} = 2000$  Oe, modelled independently as Raman (green,  $R^2 = 0.996$ ) and Orbach (blue,  $R^2 = 0.962$ ).

## 6. *Ab initio* Methods and Results

Complete-active space self-consistent field spin-orbit (CASSCF-SO) calculations were investigated using single-crystal X-ray diffraction structural coordinates performed using OpenMolcas on the Spartan computational platform. Calculations were performed using relativistic corrected ANO-RCC basis sets of triple- $\zeta$  plus polarization for lanthanide ions, double- $\zeta$  plus polarization (DZP) for coordinating atoms, and double- $\zeta$  (DZ) for all remaining atoms. The active space in **1-Ln** was the seven 4f orbitals including one electron for Ce(III), two electrons for Pr(III) and three electrons for Nd(III). State-averaging at the CASSCF level was performed for 7 doublets for Ce(III), 21 triplets and 28 singlets for Pr(III) and 35 quartets, and 112 doublets for Nd(III). The restricted active space state interaction with the spin-orbit (RASSI-SO) method included all spin-free states. An additional RAS-probing calculation labelled **1-Ce-5d** was explored including 5 orbitals in the Ras3 with 2 excitations allowed. The orbitals are determined with major contribution from the Ce-5d atomic orbitals, see Table S9.

**Table S5.** Electronic structure of **1-Ce** as calculated from CASSCF-SO calculation. Wavefunction composition under 5% are not shown.

Energy /cm <sup>-1</sup>	$g_x$	$g_y$	$g_z$	Angle /°	Wavefunction composition	$\langle J_z \rangle$
0	0.1330	0.2253	4.0521	-	0.99  $\pm 5/2$ >	2.465
532	0.6749	1.7610	2.8360	80.99	0.81  $\pm 1/2$ > + 0.15  $\pm 3/2$ >	0.572
572	0.2025	0.8311	2.6814	43.32	0.84  $\pm 3/2$ > + 0.13  $\pm 1/2$ >	1.310

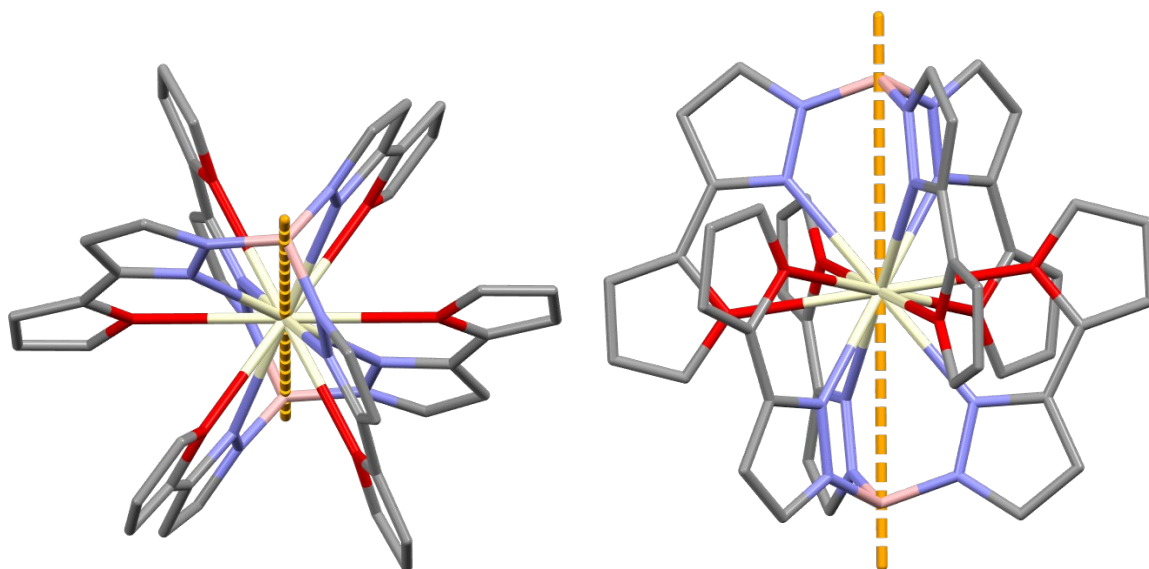


**Figure S20.** Two viewings of  $g_z$  vector (easy axis) of the ground Kramers doublet in **1-Ce**.

**Table S6.** Electronic structure of **1-Pr** as calculated from CASSCF-SO calculation. Wavefunction composition under 5% are not shown.

Energy /cm <sup>-1</sup>	$g_x$	$g_y$	$g_z$	Angle /°	Wavefunction composition	$\langle J_z \rangle$
0	0.0000	0.0000	5.9644	-	0.47 +4> + 0.47 -4>	0.0
2.34					0.48 +4> + 0.48 -4>	0.0
47.7	-	-	-	-	0.44 +3> + 0.44 -3> + 0.09 0>	0.0
141	0.0000	0.0000	2.3772	38.63	0.47 +2> + 0.47 -2>	0.0
151					0.33 -2> + 0.33 -2> + 0.12 +1> + 0.12 -1>	0.0
234	-	-	-	-	0.44 +3> + 0.44 -3> + 0.06 +2> + 0.06 -2>	0.0
551	0.0000	0.0000	1.2040	33.61	0.41 +1> + 0.41 -1> + 0.12 0>	0.0
566					0.35 +1> + 0.35 -1> + 0.12 +2> + 0.12 -2>	0.0
766	-	-	-	-	0.77 0> + 0.06 +1> + 0.06 -1> + 0.06 +3> +0.06 -3>	0.0

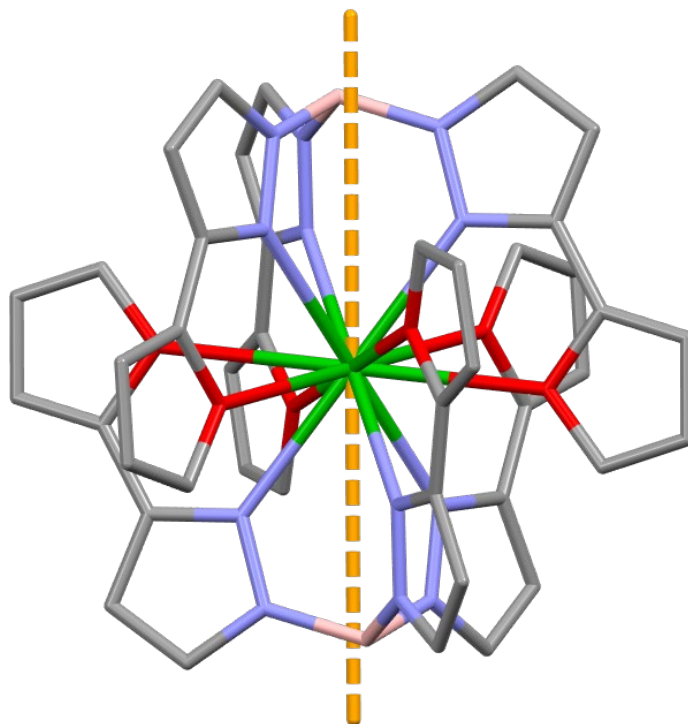


**Figure S21.** Viewing of  $g_z$  vector (easy axis) of the ground pseudo-Kramers doublet in **1-Pr**.

**Table S7.** Electronic structure of **1-Nd** as calculated from CASSCF-SO calculation. Wavefunction composition under 5% are not shown.

Energy /cm <sup>-1</sup>	$g_x$	$g_y$	$g_z$	Angle /°	Wavefunction composition	$\langle J_z \rangle$
0	0.1032	0.4016	4.8791	-	$0.67 \pm 7/2\rangle + 0.16 \pm 9/2\rangle + 0.13 \pm 5/2\rangle$	3.406
20.5	0.0006	0.0860	5.1494	16.85	$0.51 \pm 9/2\rangle + 0.22 \pm 3/2\rangle + 0.16 \pm 7/2\rangle + 0.07 \pm 5/2\rangle$	3.368
150	1.0062	1.5049	1.8242	86.83	$0.38 \mp 3/2\rangle + 0.28 \pm 5/2\rangle + 0.12 \pm 1/2\rangle + 0.08 \mp 3/2\rangle + 0.07 \pm 3/2\rangle + 0.06 \pm 7/2\rangle$	0.729
397	1.6973	2.1384	2.3275	82.54	$0.39 \pm 5/2\rangle + 0.27 \mp 1/2\rangle + 0.11 \pm 3/2\rangle + 0.08 \mp 3/2\rangle + 0.07 \pm 7/2\rangle + 0.06 \pm 1/2\rangle$	1.130
501	0.0396	0.3397	3.8146	11.43	$0.42 \pm 3/2\rangle + 0.32 \pm 9/2\rangle + 0.12 \pm 1/2\rangle + 0.12 \pm 5/2\rangle$	2.451

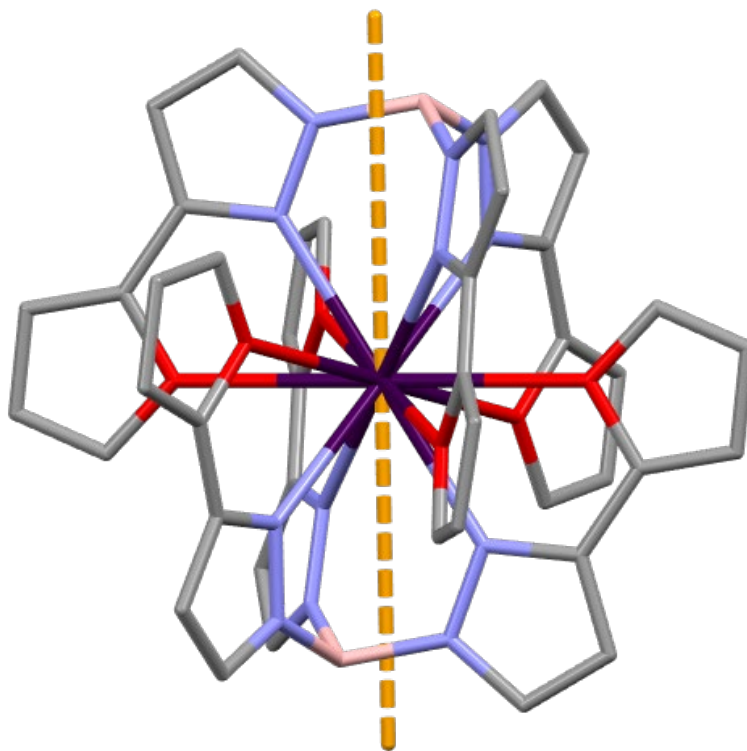


**Figure S22.** Viewing of  $g_z$  vector (easy axis) of the ground Kramers doublet in **1-Nd**.

**Table S8.** LoProp Charges on Lanthanide centres (Ln), boron and included hydride (B and H respectively), and coordinating atoms ( $N_{pz}$ ,  $O_{Fu}$ ) for **1-Ln** (Ln = Ce, Pr, Nd).

Complex	Ln	B		H	
<b>1-Ce</b>	2.4501	0.0998	0.0998	-0.0144	-0.0144
<b>1-Pr</b>	2.4539	0.0956	0.0956	-0.0065	0.0055
<b>1-Nd</b>	2.4615	0.0955	0.0953	-0.0066	-0.066

Complex	$N_{pz}$					
<b>1-Ce</b>	-0.3684	-0.3685	-0.3635	-0.3633	-0.3612	-0.3613
<b>1-Pr</b>	-0.3648	-0.3649	-0.3685	-0.3686	-0.3605	-0.3604
<b>1-Nd</b>	-0.3637	-0.3637	-0.3618	-0.3622	-0.3699	-0.3694

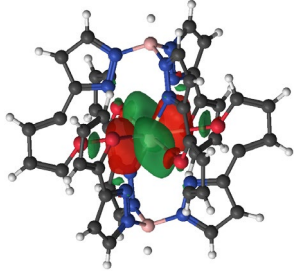
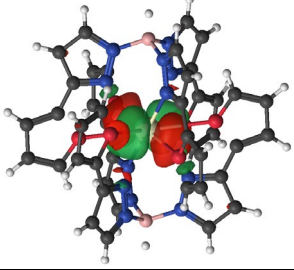
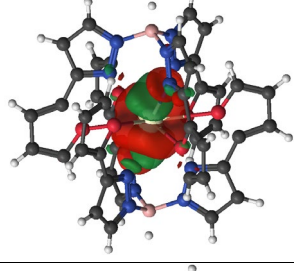
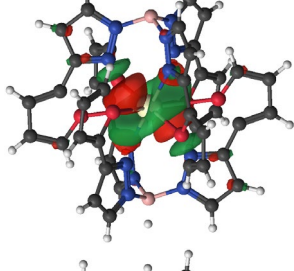
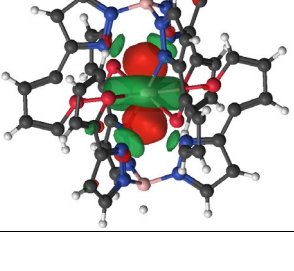
Complex	$O_{Fu}$					
<b>1-Ce</b>	-0.3478	-0.3475	-0.3493	-0.3488	-0.3423	-0.3424
<b>1-Pr</b>	-0.3485	-0.3487	-0.3503	-0.3496	-0.3437	-0.3436
<b>1-Nd</b>	-0.3489	-0.3487	-0.3414	-0.3415	-0.3504	-0.3501



**Table S9.** Electronic structure of **1-Ce-5d** as calculated from CASSCF-SO calculation with orbitals 249-253 included in the RAS3 space. Wavefunction composition under 5% are not shown.

Energy /cm <sup>-1</sup>	$g_x$	$g_y$	$g_z$	Angle /°	Wavefunction composition	$\langle J_z \rangle$
0	0.1330	0.2253	4.0521	-	0.99 ±5/2>	2.465
532	0.6749	1.7608	2.8361	80.99	0.81 ±1/2> + 0.15 ±3/2>	0.572
572	0.2027	0.8314	2.6812	43.32	0.84 ±3/2> + 0.13 ±1/2>	1.310

Orbital Number	Occupancy	Decomposition	Electron density
249	0.00	CE1 5d1+ ( 3.201) CE1 6d1+ ( 2.300)	
250	0.00	CE1 5d1- ( 2.600) CE1 6d1- ( 1.533)	
251	0.00	CE1 6s ( 1.482) CE1 5d0 ( 2.468) CE1 6d0 ( 1.468)	
252	0.00	CE1 5d2+ ( 2.398) CE1 6d2+ ( 1.411)	
253	0.00	CE1 5d2- ( 2.204) CE1 6d2- ( 1.108)	

## 7. References

1. Cotton, F. A.; Wilkinson, G. *Advanced Inorganic Chemistry*. 5th Edition, Wiley-Interscience, New York **1988**, 966-967.
2. Thomas, J.R.; Sulway, S.A., *Acta Cryst.*, **2024**, C80, 153-158.
3. Thomas J.R.; Sulway, S.A., *RSC adv.* **2021**, 11, 16158-16160.
4. Sheldrick, G. M., *Acta Cryst.*, **2015**, A71, 3-8.
5. Sheldrick, G. M., *Acta Cryst.*, **2008**, A64, 112-122.
6. Dolomanov, O.V., Bourhis, L.J., Gildea, R.J, Howard, J.A.K. & Puschmann, H., *J. Appl. Cryst.*, **2009**, 42, 339-341.